

# Revealing Fe<sub>3</sub>O<sub>4</sub> nanoparticle aggregation in aqueous suspension by nonconventional optical methods

D. CHICEA

*Physics Dept., University Lucian Blaga of Sibiu, Dr. Ion Ratiu Str. 7-9, Sibiu, 550012, Romania,*

---

A small amount of citric acid coated magnetite nanoparticles was prepared by an already classical coprecipitation method. The nanoparticles were characterized by X Ray Diffraction and by Atomic Force Microscopy. An aqueous dilution experiment was carried on several times and time variation of the refractive index of the nanofluid and of the scattered light intensity were recorded. The results are discussed in connection with aggregate formation.

(Received May 31, 2012; accepted September 18, 2013)

*Keywords:* Fe<sub>3</sub>O<sub>4</sub> Nanoparticles, X-ray diffraction, Atomic Force Microscopy, Nanoparticle aggregates.

---

## 1. Introduction

If the size of a particle decreases and falls in the range of nanometers to tens of nanometers the quantum effects can not be neglected. The result is that the nanoparticles exhibit novel magnetic, electronic, chemical and optical properties [1,2].

The nanoparticles are order of magnitude smaller than the living cells. For this reason nanoparticle structured materials have been used lately to investigate living cells or to deliver certain substances or drugs to them assuming that they produce only a minor perturbation. Several applications of nanostructured materials in biology and medicine have been developed and are presented in review papers like [3]. Warnings about the potential danger of nanoparticles in environment were issued and techniques of detection and monitoring the nanoparticle concentration are present in the literature as well [4].

The physical properties of the nanoparticles and of the nanofluids strongly depend of the size and size distribution, therefore size characterization of the samples is crucial. The Transmission Electron Microscopy (TEM) is a typical technique used in characterizing nanoparticles and nanometer to micrometer sized clusters. While it has a very good resolution the technique is expensive, time consuming, can not work in situ, therefore it can not be used in monitoring the dynamics of a process such as aggregation.

The X-ray powder diffraction technique is currently used in characterizing the nanoparticle size distribution [5]. The Scherrer equation [6] relates the full width at peak half maximum of a specific phase to the mean crystallite size of that material, considering that the nanoparticle size is the same as the crystallite size, assumption that is correct for nanoparticles.

Nanoparticle size can be assessed using the Atomic Force Microscopy (AFM) technique as well. Results of using AFM for nanoparticle sizing are presented in [7] and [8] and a comparison of the TEM with the AFM results is

presented in [9]. The technique uses very thin samples and can not be used to monitor nanoparticle aggregation dynamics because it requires scanning the sample line by line and this is time consuming, depending on the scanning resolution.

An alternative technique for nanoparticle sizing uses coherent light scattering on suspensions. The image changes in time and presents fluctuations as a consequence of the scattering centers complex movement of sedimentation and Brownian motion [10], [11]. Reference [12] reveals that the correlation function of the near-field speckle depends of the particles size. The work reported in [13] and [14] employed a transmission optical set-up and reported that speckle size and contrast are related to the average particle diameter. Ref. [15] reports a strong variation of the average speckle size and contrast with the concentration of the scattering centers. The work described here used suspensions that can have both different nanoparticle concentration and size, therefore the speckle analysis technique is not suited for particle sizing.

The physical method that exploits the correlation of the speckle dynamics with the Brownian motion is called Dynamic Light Scattering (DLS) or Photon Correlation Spectroscopy (PCS) and the physical principles of the method are explained in articles like [10 - 12]. The results on nanoparticle aggregation dynamics reported in this work are compared with previous work that used modified versions of DLS and Static Light Scattering (SLS). The Static Light Scattering technique (SLS) measures the intensity of the scattered light at many angles. The average molecular weight of a macromolecule like a polymer or a protein and the radius of gyration can be calculated. By measuring the intensity of the scattered light the calculation of the root mean square radius, also called the radius of gyration [16] is possible. A modified version of the Static Light Scattering (SLS) technique measures the light scattering anisotropy coefficient  $g$ , which strongly depends of the scattering center diameter. A functional dependence of the  $g$  parameter with the nanoparticle

diameter can be derived using Mie calculations and used to assess the nanoparticle diameter [17], [18].

Other class of nanoparticle characterization techniques uses magnetization. In single-domain particle systems after magnetization both Brownian and Neel type of relaxation processes are possible. The Brownian relaxation time depends on viscosity of the carrier liquid and of the hydrodynamic radius  $r$  of the particle [19] while the Neel time relaxation depends of the particles by the effective anisotropy constant and by the mean magnetic volume of the particles [19]. Ferromagnetic resonance provides information on the effective anisotropy constant and on the anisotropy field [20]. Moreover, information regarding the colloidal stabilization of the magnetic particles in the presence of an external field is an outcome of the ferromagnetic resonance technique, as well [20].

When diluted in aqueous solution (as the body fluids are) the nanoparticles aggregate very fast [8,17,18,21]. The former nanofluid quickly exhibits micron sized particles in suspension. As the rheological properties of the nanofluid strongly depend of the nanoparticles size distribution and concentration, it is of interest for biomedical applications to know the time scale of the aggregation process.

The following sections describe the recipe used in preparing Fe<sub>3</sub>O<sub>4</sub> nanoparticles in aqueous suspension, the results of the X Ray diffraction and AFM characterization. The time variation of the refractive index and the intensity of the scattered light variation during aqueous dilution are presented as well and the results are discussed in connection with previous experimental work performed on nanoparticle aggregation monitoring using DLS and SLS.

## 2. Nanofluid synthesis

The procedure we used to prepare the aqueous nanofluid is a typical coprecipitation. The reagents used were: FeCl<sub>2</sub>·4H<sub>2</sub>O, FeCl<sub>3</sub>·6H<sub>2</sub>O, ammonium hydroxide (NH<sub>3</sub>[aq]), citric acid (C<sub>6</sub>H<sub>8</sub>O<sub>7</sub>), produced by Merck. Double deionised water was used to dissolve the reagents.

The solutions were prepared right before synthesis, in order to prevent their contamination with atmospheric oxygen. First 10.44g of FeCl<sub>3</sub>·6H<sub>2</sub>O and 4.16 g of FeCl<sub>2</sub>·4H<sub>2</sub>O, were dissolved in 0.380 l of double deionised water. The temperature brought to 75°C and maintained at this value while continuously stirring the solution. 40 ml of 25% ammonium hydroxide were slowly added, one drop at a time. A black precipitate (magnetite Fe<sup>2+</sup>Fe<sup>3+</sup><sub>2</sub>O<sub>4</sub>) was formed during the slow addition and was forced to sediment using a strong magnet.

The magnetite was rinsed three times by adding deionised water at 50 °C, using the magnet to settle the magnetite, and discarding the clear water, to completely remove the excess ammonium hydroxide from the particles. At the end of this stage of the preparation process the solution pH was 7.5.

At this stage of the synthesis the nanoparticles were stabilized by adding 1 mL of the 42% citric acid and mixing the ferrofluid for 2 minutes by moving the beaker

over the magnet while maintaining the temperature at 80°C.

Overall the chemical reaction was:



Again excess solution was discarded. The output was a viscous, black fluid. The volume fraction  $\phi$  of nanoparticle phase in the nanofluid sample was calculated using mass density measurements using Eq. (2):

$$\phi = \frac{\rho_f - \rho_l}{\rho_s - \rho_l} \quad (2)$$

where  $\rho_f$  is the density of the ferrofluid,  $\rho_l$  the density of the carrier fluid and  $\rho_s$  the density of the solid particles. Density was measured using a picnometer at  $T = 293\text{K}$ . Using (2) we found that the volume fraction  $\phi$  of nanoparticles was 8.23%. The nanofluid obtained using this procedure remained stable for 20 month that passed since producing it till writing the manuscript of this article.

The recipe and the procedure used in manufacturing the nanofluid are different from the simple procedure reported in [22] as the temperature was not maintained constant at 20°C but was carefully monitored, controlled and maintained at 75°C during the co-precipitation stage of the synthesis. The reason for changing the recipe is that the nanofluid produced in the work reported in [22] had brown and red reflexes, indicating the presence of maghemite. Reference [23] using TEM reports that by using a temperature range of 65-75 °C, the procedure will produce spherical magnetite nanoparticles. References [24] and [25] reveal the influence of the temperature on the shape and size distribution of the nanoparticles produced by coprecipitation.

The nanofluid we obtained was black and did not exhibit red or brown reflexes, meaning that the nanoparticles were magnetite (Fe<sub>3</sub>O<sub>4</sub>) not maghemite ( $\gamma\text{-Fe}_2\text{O}_3$ ) and is the same batch that was used in the work described in [26], which contains more details on the synthesis procedure.

The following section describes the X ray power diffraction and the AFM procedures used in investigating the nanoparticle size distribution.

## 3. Nanoparticles characterization

### 3.1 Powder X ray diffraction

A small amount (0.5 ml) of the liquid sample produced following the procedure described in the previous section was placed in a Petri dish, maintained at 85 °C for 2 hours and became a black solid sample. The powder X-ray diffraction (XRD) patterns were obtained with a Bruker D8 Advance powder diffractometer working at 40 kV and 40mA, using CuK $\alpha$  wavelength, with a Germanium monochromator and were used for crystal phase analysis. The measurement was performed in the

range angle  $2\theta=15-85^\circ$  and in a step-scanning mode with a step  $\Delta 2\theta = 0.01^\circ$ .

Phase analysis was carried out using the PowderCell software [27]. The microstructural information obtained were the effective crystallite mean size,  $D_{\text{eff}}$  (nm) and the root mean square (rms) of the microstrains,  $\langle \epsilon^2 \rangle^{1/2}_m$ , [28]. The Warren-Averbach X-ray Fourier analysis peak profiles were processed by the XRLINE computer program [29]. More details on the X-ray diffraction experiment and data processing are presented in [26].

The XRD diffraction pattern, presented in [26], reveals that the sample is magnetite  $\text{Fe}_3\text{O}_4$  – cubic crystalline structure phase [30]. The effective crystallite mean size distribution function  $D(L)$  for the magnetite sample [26] reveals a broad distribution of the crystallites dimensions with a mean value of 10.9 nm.

The results of the powder diffraction experiment are similar with the results reported in the literature regarding X ray powder diffraction on  $\text{Fe}_3\text{O}_4$  nanoparticles, [31] being just one of them.

### 3.2. AFM nanoparticle characterization

The atomic force microscope (AFM) is a scanning probe microscope that uses a flexible cantilever to measure the force between the tip and the sample. The local attractive or repulsive force between the tip and the sample is translated into a deflection of the cantilever. The cantilever is attached to a rigid substrate and will deflect towards or away from the surface [32] according to the sample topography.

The optical lever principle is used; a small change in the bending angle of the cantilever is converted to a precisely measurable deflection in the position of the reflected spot. A topography image of the surface is reconstructed by the software that drives the scanning process.

The AFM that was used in the work reported here is an Agilent 5500 type. The scanning mode was ACAFM. A soft tip with the spring constant equal to 5 N/m was used at low force amplitude.

Sample preparation is crucial in order to get useful AFM images [8]. Samples must be thin enough and must adhere well to the surface, otherwise the scanning process will producing artifacts. More details are presented in [8] and [33].

Sample preparation involved depositing a drop of nanofluid on mica substrate and stretching with a blade to form a very thin layer, thin enough to have only one layer of nanoparticles after solvent evaporation. The mica substrate was freshly cleaved in order to have a clean surface with atomic grade plane. The thin layer was left for 3 hours to evaporate. More details on sample preparation and scanning procedure are presented in [8] and [33].

Several scans were carried on selecting an area on the surface having individual nanoparticles. Aggregates were present as well. A bigger resolution scan, (512x512 pixels) of an area covering  $0.5 \mu\text{m} \times 0.5 \mu\text{m}$  was carried on and the topography is presented in Fig. 1.

Examining Fig. 1 we notice several nanoparticles located on the scanned area. We also notice the bright spot on the upper part of the image, corresponding to the highest location of the scan, at 63 nm upper than the substrate. This reveals that the nanofluid was not free of aggregates. The scans of other location did not exhibit such big particles, indicating that aggregates are rare though.

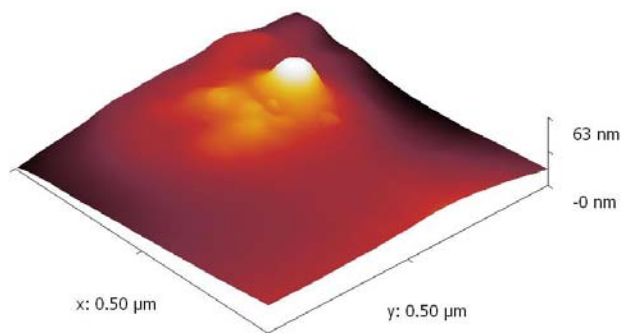


Fig. 1 The 3D topography of the evaporated nanofluid. Z axis is in nm.

Profiles extracted from the 3D images can produce more accurate information than the 3D topography views. Fig. 2 and 3 present several profiles extracted over nanoparticles.

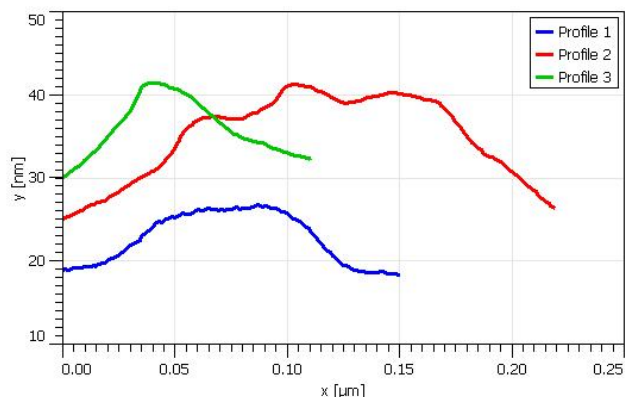


Fig. 2 Profiles extracted over nanoparticles

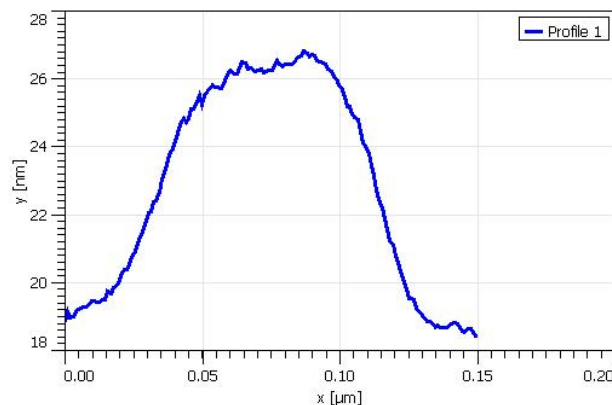


Fig. 3 Another profile extracted over a nanoparticle

The difference between the top and the base line values of the curves indicate the size of the nanoparticle. Figs. 2 and 3 reveal that the size of the nanoparticles is around 8 – 15 nm, which is consistent with the XRD average grain size of 10.9 nm and with the DLS nanoparticle sizing experiment results on samples from the same nanofluid reported in [26].

Several samples from the nanofluid that was produced and that has the nanoparticle physical properties presented in this section were subject to an aqueous dilution experiment aiming to monitor the aggregation process dynamics and the results are presented in the next sections.

#### 4. Refractive index measurements

An aqueous dilution experiment was conducted aiming to monitor the time variation of the refractive index of the solution. As the concentrated Fe<sub>3</sub>O<sub>4</sub> nanofluid is opaque, a smaller concentration nanofluid was prepared. A DRC-200 Abbe type digital refractometer placed in a setup to produce one measurement every 0.9 s was used for measuring the refractive index. The resolution of the refractometer is 0.0001. The refractometer display was optically recorded during the experiment and the refractive index variation in time was extracted later on and more details on the technique are presented in [26].

The temperature of the environment where the measurements were carried on was 23.4 °C. Very small amounts of solvent and nanofluid were used: 0.4 ml of deionized water and 0.02 ml of nanofluid, prepared as described in section 2. The deionized water was placed in the open sample location of the refractometer. The small amount of nanofluid was first aspirated in a 0.1 ml syringe and injected in the deionized water. Recording was started 6 seconds prior of nanofluid injection and this constant part prior of nanofluid injection is not presented in Fig. 4, which presents the time variation of the refractive index during nanofluid dilution in deionized water. The 0 on the time axis was shifted to match the beginning of the nanofluid injection.

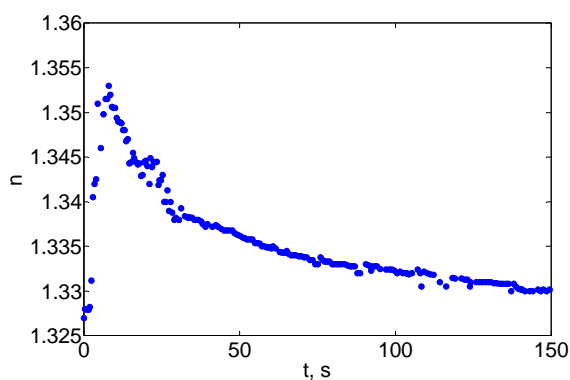


Fig. 4 The time variation of the refractive index of the diluted nanofluid.

Fig. 4 reveals a fast increase of the refractive index during the first 10 seconds of the dilution process. This

time interval is consistent with the time required for the diluted nanofluid to get homogenized by the convection currents produced by injection. The refractive index of the diluted nanofluid is bigger than the index of the deionized water, because the suspension, the ferrite nanoparticles, has a bigger refractive index, around 1.6, typical for glassy substances.

As time passes, a fast aggregation occurs in the diluted aqueous nanofluid, as presented in [17,18,21,34]. The number of aggregates is much smaller than the number of nanoparticles and this explains the decrease in the refractive index of the diluted nanofluid. The decrease was fast for about 20 s and slow for another 100 s. The fast decrease time span is consistent with the aggregation time reported in [18] and [21]. The aggregation time depends both of the temperature and of the geometry of the cuvette where the process carries on, therefore time differences of several seconds are quite normal. Nevertheless, the final refractive index of the diluted nanofluid is 1.3320, slightly bigger than 1.3270 that was measured for the deionized water sample used for dilution.

The sedimentation velocity increases with the square of the radius of the particle, in a laminar flow regime. This can be derived easily by equaling to zero the buoyant force, gravity and Stokes force after reaching steady motion regime. When particles increase from 10 nm to 1.2 μm the sedimentation can no longer be neglected [35]. The slow decrease during the last 130 s can be explained by the decrease of the number of aggregates in the refractometer measuring volume caused by sedimentation.

#### 5. Scattered light intensity measurements

In a nanofluid coherent light scattering is done by small particles, with size comparable with the wavelength or smaller, therefore the Rayleigh approximation can be used to describe the process [36]. When the aggregation process carries on, the average aggregate diameter  $d$  increases. Assuming that  $d$  is the average particle (whether nanoparticle or aggregate) diameter, the total number of particles in suspension  $N$  varies with the diameter  $d$  as:

$$N = \frac{V_{nano}}{\frac{4\pi}{3} \cdot \left(\frac{d}{2}\right)^3} \quad (3)$$

where  $V_{nano}$  is the total nanoparticle volume in suspension, a constant value. The light intensity scattered by a single particle  $\langle I_n(\theta) \rangle$  is proportional to  $d^6$  [16], as described by Rayleigh approximation. The average intensity  $\langle I(\theta) \rangle$  scattered by all the nanoparticles in the sample at a certain angle is therefore proportional to  $d^3$ , as described by eq. (4), thus rapidly increasing with the aggregates diameter.

$$\langle I(\theta) \rangle \sim N \cdot \langle I_n(\theta) \rangle \sim d^3 \quad (4)$$

Moreover, using eq. (4) we notice that the light intensity scattered by one aggregate having a diameter around one micron is roughly  $10^6$  times bigger than the intensity scattered by one nanoparticle with a diameter around 10 nm, therefore the far field aspect is dictated by light scattered on aggregates, once as they are formed.

The fast increase of the average light scattered intensity (4) with the diameter suggests a simple procedure for a half-quantitative assessment of the degree of nanoparticle aggregation. A coherent light beam is incident on a cuvette containing deionized water, located within the coherence length. A detector and a data acquisition system are placed after the cuvette (a forward light scattering experiment) at a small angle and the intensity of the scattered light is recorded during the dilution process. A typical setup is presented in Fig. 5 and is the same setup used in previous work on light scattering on suspensions [15] and on DLS characterization [8], [21], [22].

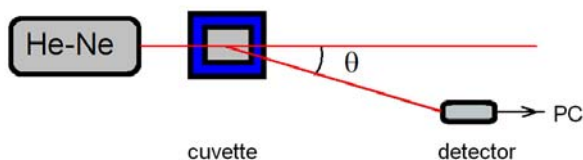


Fig. 5. Light scattering setup, view from above.

The light source was a laser diode working in continuous regime at a constant power of 18 mW. The wavelength of the laser beam was 635 nm. The experiment was conducted at 20 °C. The cuvette-detector distance  $D$  was 0.46 m and the detector was set 0.036 m aside from the beam, therefore the scattering angle  $\theta$  was equal to  $4^\circ 28' 29.63''$ .

A volume of 0.01 ml concentrated nanofluid was placed into a 5 ml syringe and the needle was attached. Then 4.0 ml of deionised water was aspirated into the syringe from the cuvette and a time series recording started at same time. The mixture was injected fast into the cuvette producing turbulences. The part of the time series lasting from the beginning till the fluid was mixed inside the syringe was removed. The data acquisition rate was 100Hz and was high enough to monitor the time variation of the intensity. A time series recording during such a dilution experiment is presented in Fig. 6.

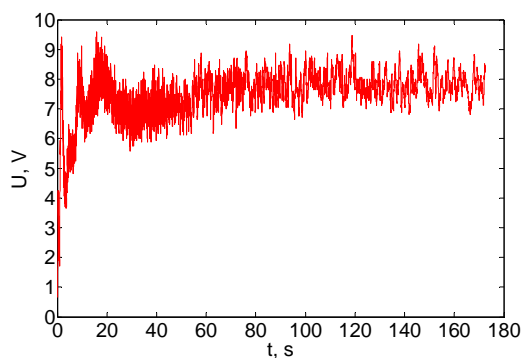


Fig. 6. The scattered light intensity variation after dilution.

Examining Fig. 6 we notice the increasing trend of the curve during the first part of over the 170 seconds, overlapped with the fast oscillations of the intensity, which are consistent with the speckle aspect mentioned earlier. We also notice that the oscillations have a bigger frequency at the beginning of the recording and the frequency decreases in time. This again is consistent with the DLS theory, because during the first seconds there still exist a big number of nanoparticles leading to fast fluctuation of the scattered light intensity. As the aggregates number increases, the far field aspect is dominated by light scattered on aggregates and the fluctuations have a smaller frequency. These particularities are exploited by DLS to produce the average particle size [21], [22].

Fitting a curve on the time series in Fig. 6 is time consuming and might turn to be irrelevant because the amount of data can became huge, especially if a high data acquisition rate is used and because of the speckle aspect that leads to fluctuations in the time series. A convenient alternative is to perform averages on a certain small time interval and to fit a curve on the averaged time series. Several time intervals from 0.03 to 1.5 s were used and finally the time interval of 1 s was chosen. Fig. 7 presents the variation of the averaged scattered light intensity with averages made on 1 s (circles).

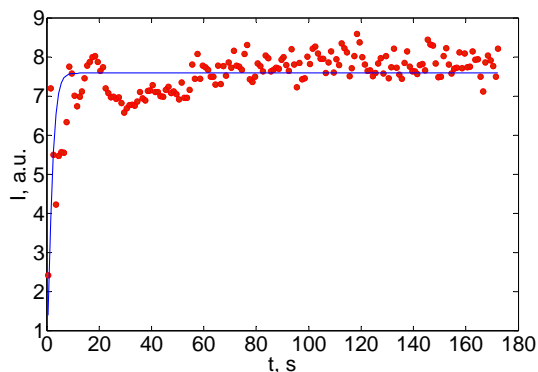


Fig. 7. The averaged scattered light intensity versus time. Averages are made on 1 s (circles) and the fit (solid line).

A simple function can be fit to the data to describe in a unitary manner the fast increase followed by a plateau. A possible function having two parameters might be the one described by eq. (5):

$$I(t) = a \cdot \tanh(b \cdot t) \quad (5)$$

In (5)  $a$  parameter acts linearly, simply scaling the function to match the plateau level. The  $b$  parameter acts non-linearly describing the fast increase of the average intensity: the bigger the  $b$  value is, the faster is the increase of the function towards reaching the plateau.

The function described by eq. (5) was fit on the averages made on 1 s using a least square minimization procedure. The values of the parameters that provided the best fit were:  $a=7.584$  and  $b=0.336$ .

This procedure is quite simple compared with the typical DLS technique that requires recording the scattered light intensity with an array of detectors and processing the data. Even the simplified version described in previous work [8], [21], [22] required a complex data processing procedure with slicing and fitting a Lorentzian function in the batch mode on each slice. Following the procedure described in this section the value of the  $b$  parameter can be found and can be a measure of the aggregation kinetics. We notice that the fast increase of the average scattered light intensity lasted for 20 seconds and was followed by a plateau that has fluctuation overlapped on it.

## 6. Discussions and conclusion

A simple recipe for preparing Fe<sub>3</sub>O<sub>4</sub> nanoparticles in aqueous suspension is presented in the first section. The nanoparticles were characterized by powder X Rays Diffraction and by Atomic Force Microscopy.

The XRD diffraction pattern illustrates that the sample obtained in our synthesis conditions is magnetite Fe<sub>3</sub>O<sub>4</sub> - cubic crystalline structure phase and that that the crystallite mean size was 10.9 nm, hence the size of the nanoparticles, assuming that the effective crystallite mean size is the same as the physical size of the nanoparticles.

The AFM technique uses an image reconstruction from successive lines acquired during a scan of the surface. Several profiles were extracted from the topography of the surface and the particle dimension was assessed from the profile. The cantilever is a consumable in the AFM technique, as the tip wears out during scanning, by becoming less sharp, therefore having a bigger tip radius [33], which requires special precautions [8]. Nevertheless, the nanoparticle size assessed by AFM is consistent with the results of the XRD techniques.

Two simple optical procedures were proposed for monitoring the nanoparticle aggregation process in diluted aqueous suspensions. The first procedure involves a precise and repeated measurement of the refractive index of the suspension after dilution. The refractive index exhibits a fast increase during homogenization followed by a fast decrease and then a slow decrease. The fast decrease corresponds to the aggregates formation in the suspension and lasted for about 20 s.

The second procedure relies on the Rayleigh scattering approximation and requires recording the scattered light intensity at a small scattering  $\theta$  angle and averaging the fluctuations. The increase of the averaged scattered light intensity corresponds to the aggregates formation and was found to last for about 20 s, consistent with the time interval found using the first procedure.

The experimental conditions for dilution were similar with those reported in previous work using DLS [8], [17], [18], and a modified version of SLS [17], [18] and so are the time intervals assessed for aggregates formation, therefore we can conclude that these two simple optical procedures could be used in nanoparticle aggregation monitoring during aqueous dilution.

## Acknowledgement

I am grateful to Dr. Emil Indrea of I.N.C.D.T.I.M Cluj-Napoca for performing the powder X-ray diffraction, for interpreting the results and for the fruitful discussions, as well.

## References

- [1] V.V. Agrawal, G.U. Kulkarni, C.N.R. Rao, *J. Phys. Chem. B* **109**, 7300 (2005)
- [2] W.C. Lin, P.C. Huang, K.J. Song, M.T. Lin, *Appl. Phys. Lett.* **88**(153), 117 (2006)
- [3] O.V. Salata, *Journal of Nanobiotechnology*, **2**(3), doi:10.1186/1477-3155-2-3. (2004).
- [4] G. G. Leppard, *Current Nanoscience* **4**(2), 278 (2008).
- [5] A. W. Hull, A new method of chemical analysis, *J. Am. Chem. Soc.*, **41**(8), 1168 (1919), doi: 10.1021/ja02229a003
- [6] A. L. Patterson, The Scherrer Formula for X-Ray Particle Size Determination *Phys. Rev.* **56**(10), 978 (1939), doi:10.1103/PhysRev.56.978.
- [7] F. Zhang, S.W. Chan, J. E. Spanier, E. Apak, Q. Jin, R. D. Robinson, I. P. Herman, *Appl. Phys. Lett.* **80**, 27 (2002); doi:10.1063/1.1430502.
- [8] D. Chicea, *Optoelectron. Adv. Mater. – Rapid Commun.* **4**(9), 1310 (2010).
- [9] L. M. Lacava, B. M. Lacava, R. B. Azevedo, Z. G. M. Lacava, N. Buske, A. L. Tronconi, P. C. Morais, *Journal of Magnetism and Magnetic Materials*, **225**(1-2), 79 (2001).
- [10] J.W. Goodman, Laser speckle and related phenomena, Vol.9 in series Topics in Applied Physics, J.C. Dainty, Ed., Springer-Verlag, Berlin, Heidelberg, New York, Tokyo, (1984).
- [11] J. D. Briers: Laser Doppler, speckle and related techniques for blood perfusion mapping and imaging, *Physiol. Meas.* **22**, R35 (2001).
- [12] M. Giglio, M. Carpineti, A. Vailati and D. Brogioli, *Appl. Opt.* **40**, 4036 (2001).
- [13] Y. Piederrière, J. Cariou, Y. Guern, B. Le Jeune, G. Le Brun, J. Lotrian, *Optics Express* **12**, 176 (2004).
- [14] Y. Piederrière, J. Le Meur, J. Cariou, J.F. Abgrall, M.T. Blouch, *Optics Express* **12**, 4596 (2004).
- [15] D. Chicea, *European Physical Journal Applied Physics* **40**, 305 (2007), DOI: 10.1051/epjap:2007163
- [16] B. H. Zimm, Molecular Theory of the Scattering of Light in Fluids. *J. Chem. Phys.*, **13**(4), 141 (1945), doi:10.1063/1.1724013.
- [17] D. Chicea, *J. Optoelectron. Adv. Mater.* **12**(1), 152 (2010).
- [18] D. Chicea, *Current Nanoscience* **8**(2), 259 (2012).
- [19] I. Malaescu, C. N. Marin, *Journal of Magnetism and Magnetic Materials* **218** (1), 91 (2000).

- [20] I. Malaescu, C. N. Marin, *Physica B: Condensed Matter* **365**(1-4), 134 (2005).
- [21] D. Chicea, *Optoelectron. Adv. Mater. – Rapid Commun.* **3**(12), 1299 (2009).
- [22] D. Chicea, C. M. Goncea, *Optoelectron. Adv. Mater. – Rapid Commun.* **3**(3), 185 (2009).
- [23] G. F. Goya, T. S. Berquo, F. C. Fonseca, M. P. Morales, *Journal of Applied Physics* **94**, 3520 (2003).
- [24] Z.L Liu, Y.J. Liu, K.L. Yao, Y.H. Ding, J. Tao, X. Wang, *Journal of Materials Synthesis and Processing* **10**, 83 (2002).
- [25] L. Vayssieres, C. Chaneac, E. Tronc, J. P. Jolinet, *Journal of Colloid and Interface Science* **205**, 205 (1998).
- [26] D. Chicea, E. Indrea, C. M. Cretu, *J. Optoelectron. Adv. Mater.* **14**(5-6), 460 (2012)
- [27] W. Kraus, G. Nolze, *POWDER CELL J. Appl. Crystallogr.* **29**, 301 (1996).
- [28] E. Indrea, Adriana Barbu, *Appl. Surf. Sci.*, **106**, 498 (1996).
- [29] N. Aldea, E. Indrea, *Comput. Phys. Commun.* **60**, 155 (1990).
- [30] R. T. Downs, M. Hall-Wallace, *American Mineralogist*, **88**, 247 (2003).
- [31] J. Wan, G. Tang, y. Qian, *Appl. Phys. A* **86**, 261 (2007)
- [32] <http://www.jpk.com/general-scanning-probe-microscopy.431.html>
- [33] D. Chicea, B. Neamtu, R. Chicea, L. M. Chicea, *Digest Journal of Nanomaterials and Biostructures* **5**(4), 1015 (2010).
- [34] D. Chicea, *Journal of Optoelectronics and Advanced Materials* **12**(4), 858 (2010).
- [35] D. Chicea, *Applied Optics* **47**(10), 1434 DOI: 10.1364/AO.47.001434.
- [36] Bohren C.F.; Huffman D. *Absorption and scattering of light by small particles*, John Wiley, New York, (1983).

---

\*Corresponding author: dan.chicea@ulbsibiu.ro